AMERICAN ACADEMY OF OPHTHALMOLOGY®

Longitudinal Imaging of the Parafoveal Cone Mosaic in Congenital Achromatopsia

Nickolas Chen, MD,[1,] Katie M. Litts, PhD,[2,*,†] Danica Nikezic, BS,[2] Christopher S. Langlo, MD, PhD,[2] Brian P. Higgins, BS,[2] Byron L. Lam, MD,[3] Gerald A. Fishman, MD,[4] Frederick T. Collison, OD,[5,6] Mark E. Pennesi, MD, PhD,[7,8] Christine N. Kay, MD,[9] Sergey Tarima, PhD,[10] Joseph Carroll, PhD[2,11]*

Purpose: To assess longitudinal changes in parafoveal cone density in individuals with congenital achromatopsia (ACHM).

Design: Retrospective longitudinal study.

Participants: Nineteen individuals (7 women and 12 men) with genetically confirmed ACHM. To be eligible, each had adaptive optics scanning light ophthalmoscope (AOSLO) images of the photoreceptor mosaic from ≥2 time points.

Methods: For each individual, follow-up AOSLO montages were aligned to their baseline montage. Notably, 100 × 100 μm regions of interest (ROIs) were extracted from the split-detection modality at locations 1°, 5°, and 10° temporal (T) from the peak cone density in each montage. All ROIs from follow-up visits were then manually aligned to their respective baseline ROI for that location. Cones were identified in each ROI by one observer, reviewed by a second observer, and confirmed together in a masked fashion. Cone density was calculated, and a linear mixed model was used to assess changes in density over time. A Wald test was performed to determine if the cone density changes were statistically significant.

Main Outcome Measures: Parafoveal cone spacing (at 1°, 5°, and 10° T) as a function of time.

Results: The mean (± standard deviation [SD]) age at baseline was 21.6 ± 10.7 years and the mean (±SD) follow-up period was 3.83 ± 2.93 years (range, 0.46–8.66 years). At 1° T, we observed a significant decrease of 352 cones/mm^2 per year ($P = 0.0003$). At 5° T, the linear mixed model showed a nonstatistically significant decrease of 58 cones/mm^2 per year ($P = 0.504$). At 10° T, we observed a significant decrease of 139 cones/mm^2 per year ($P = 0.0188$). For a 100 × 100 μm ROI, these density changes correspond to a reduction of between about 0.5 and 4 cones per year, depending on the location.

Conclusions: Parafoveal cone density estimates in ACHM show a small decrease over time. These observed changes are within the previously reported longitudinal repeatability values for normal retinas, suggesting the observed average cone loss may not be clinically meaningful. Further studies with longer follow-up times and more genetically heterogeneous and age-diverse populations are needed to better understand factors contributing to changes in foveal and parafoveal cone structure in ACHM over time.

Financial Disclosure(s): Proprietary or commercial disclosures may be found in the Footnotes and Disclosures at the end of this article. *Ophthalmology Science 2025;5:100765*

Supplemental material available at www.ophthalmologyscience.org.

Congenital achromatopsia (ACHM) is a retinal disorder associated with substantially reduced or absent cone function, severely impaired or absent color vision, nystagmus, photophobia, and reduced visual acuity. Achromatopsia has been linked to mutations in 6 genes (*CNGA3*, *CNGB3*, *GNAT2*, *PDE6C*, *PDE6H*, and *ATF6*), with approximately 70% of cases associated with *CNGA3* and *CNGB3* mutations.[1–4] The success of gene therapy trials aimed at restoring cone function in patients with ACHM hinges on the presence of remnant cones in the retinas of these patients. Imaging with an adaptive optics scanning light ophthalmoscope (AOSLO) allows for noninvasive assessment of remnant cone structure in ACHM.[5–7] Marked interindividual variation in foveal cone density has been reported in patients with ACHM,[7,8] which supports the idea that there may be different therapeutic potential across individuals. Of additional interest is using AOSLO to assess cone structure after administration of gene therapy, which could provide a sensitive measure of treatment response as well as serve as a possible safety measure. Having an accurate assessment of the natural history of disease in these patients is crucial to interpreting AOSLO data after therapeutic intervention.

There is conflicting evidence regarding stability of foveal cone structure in ACHM. Using OCT to assess foveal outer nuclear layer (ONL) thickness, Thiadens et al[9] showed that retinal thickness correlated with age, whereas Thomas

https://doi.org/10.1016/j.xops.2025.100765
ISSN 2666-9145/25

et al[10] reported that ONL thickness decreased in younger patients but remained unchanged in other patients. However, other cross-sectional studies have found no association between ONL thickness and age.[7,8,11] Longitudinal studies of ONL thickness showed similar disagreement. Aboshiha et al[12] and Grissim et al[13] both reported no significant change in ONL thickness at the fovea over an average 1.6 and 3.1 year follow-up, respectively. In contrast, 2 other studies[14,15] showed a slight increase in ONL thickness over an average 1.07 and 5.1 years follow-up, respectively. OCT has also been used to examine the integrity of the ellipsoid zone (EZ), with most cross-sectional studies reporting more severe EZ phenotypes with increasing age,[9,10] although Sundaram et al[11] found no significant association between EZ grade and age. Longitudinal studies are emerging, and, although EZ structure has been shown to be remarkably stable in most patients (with up to 5 years follow-up in some patients), there are some patients with clear changes in EZ structure over time (between 5% and 17% of patients in various studies).[12–16] In contrast, Triantafylla et al[17] showed changes in EZ structure at the fovea in 15 of 17 patients (88%) but showed no significant change in ONL thickness over an average of 5.7 years follow-up. Using AOSLO images to examine remnant inner segment structure at the fovea, Georgiou et al[8] showed a weak negative association between age and peak cone density in a cohort with only *CNGA3*-associated ACHM, whereas studies in a *CNGB3*-associated ACHM cohort showed no association between age and peak foveal cone density.[7,14] Longitudinal AOSLO studies have reported relatively stable foveal cone structure in both *CNGA3*-associated[18] and *CNGB3*-associated ACHM.[14]

Beyond the conflicting conclusions from the above studies, another limitation is that studies to date have focused almost exclusively on foveal cone structure. Although this is thought to be the area with the greatest potential to restore visual function in patients with ACHM, it makes up a relatively small area overall, especially with respect to the blebs typically used to deliver viral vector.[19] Thus, it is important to have similar natural history data on parafoveal cone structure. Additionally, there is considerable variation in rod:cone ratios throughout the retina,[20] and therefore it is possible that the remnant foveal and parafoveal cones might have different fates in patients with ACHM. Therefore, the purpose of this study was to longitudinally examine the parafoveal cone mosaic in patients with ACHM.

Methods

Participants

The research study was approved by the Institutional Review Board at the Medical College of Wisconsin (PRO00027165) and followed the tenets of the Declaration of Helsinki. Written informed consent was obtained from all individuals and their information stored in a database (Lattice Version 1.0, Translational Imaging Innovations, Inc). Nineteen individuals with genetically confirmed ACHM and ≥1 follow-up visit where an AOSLO montage was generated were included in this study. Most of these individuals were previously enrolled in a natural history study (NCT1846052), as summarized in Table S1 (available at www.ophthalmologyscience.org).

AOSLO Imaging and Analysis

The eye with the best image quality for each individual was imaged at multiple time points using a custom built AOSLO at the Medical College of Wisconsin as previously described.[7,21,22] Before imaging, individuals had their pupil dilated and cycloplegia was induced with 1 drop each of 1% tropicamide and 2.5% phenylephrine or 1 drop of Cyclomydril only. In brief, a 775 or 790 nm light source was used for imaging and an 850 nm light source was used for wavefront sensing. A dental impression on a bite bar was used to stabilize the head during imaging. Confocal and nonconfocal split-detector AOSLO images focused on the cone mosaic were acquired simultaneously (i.e., with spatial and temporal coregistration) as previously described.[7] Image sequences consisting of 150 to 200 frames with an acquisition rate of 16.6 frames/s were recorded at different retinal locations using a fixation target. The imaging protocol included a 5° × 5° square grid centered on the fovea and a 12° × 1.75° strip of images collected temporally (T) from the fovea, sampled at 1° intervals using 1° to 1.75° square fields of view. In addition to this standardized imaging protocol, the baseline montage was overlayed on a fundus image and made available to the imaging team during acquisition to help ensure the same retinal images were captured (although the fundus image was not consistently used).

The raw frames from each image sequence underwent static sinusoidal distortion correction and were strip-registered to an automatically selected reference frame, as previously described.[23] Confocal and split-detector AOSLO images were montaged simultaneously either manually or semiautomatically using a multimodal montaging algorithm[24] and Adobe Photoshop CS6 (Adobe Systems, Inc). The linear scale of the AOSLO images for a given individual ($S'_{R(x)}$; units: μm/pixel) was estimated at each time point using the following equation:

$$S'_{R(x)} = \frac{T}{f_l T_s}\left(\frac{180}{\pi}\right) RMF\left(\frac{l_A}{l_{A,0}}\right)$$

where T represents the periodicity of a Ronchi ruling (μm/cycles), f_l represents the focal length of the model eye in our system (μm), T_s represents the sampling period of the lines in the model eye image of the Ronchi ruling (pixels/cycle), RMF represents the assumed retinal magnification factor (291 μm/degree) of an eye with a 24.0 mm axial length (represented $l_{A,0}$), and l_A represents the actual axial length of the individual's eye in mm (measured with an IOL Master, Carl Zeiss Meditec, Inc.).[21]

Imaging, image processing, and image montaging were performed at each study visit. For each individual's baseline montage, the location of peak cone density within the rod-free zone was estimated as previously described.[7,21] Using the individual's baseline image scale as described above, all follow-up montages were scaled to the baseline AOSLO montage and manually aligned to the baseline montage using blood vessel features in the confocal modality (Adobe Photoshop CS6, Adobe Systems, Inc). The manual alignment of the montages was further refined by cone-to-cone alignment between the split-detector AOSLO montages. Next, split-detector images within each parafoveal locations (1°, 5°, and 10° T to the location of peak cone density) were manually selected based on subjectively good image quality (defined as sufficient to assess remnant cone structure), absence of blood vessels, and degree of overlap between the baseline and all the follow-up visits (assessed by author N.C.). All selected image

layers were repaired for eye motion (https://github.com/OCVL/Eye-Motion-Repair).[25] Next, to account for apparent misalignments in cone locations due to differences in image distortion between imaging sessions, the selected follow-up images were aligned to the baseline image using an affine transformation of the "Adaptive Optics Align" mode in i2k Retina (DualAlign). To accurately align the selected follow-up images to baseline, cones in the baselines image were manually identified and selected as a reference point, then corresponding cones were manually identified and selected at each follow-up image in i2k Retina. The aligned and transformed output images from i2k Retina were then manually realigned to the baseline montage and a 100 μm × 100 μm region of interest (ROI) was manually extracted using Adobe Photoshop CS6 at each location of interest and time point for analysis.

The ROIs were masked for individual, retinal location, and time. Cones were then semiautomatically identified using Mosaic Analytics (Translational Imaging Innovations) in each ROI by one observer (J.C.). The cones identified by observer 1 were reviewed by a second observer (N.C.). All ROIs were then rereviewed together with both reviewers until consensus of cone identification was reached. Bound cone density was calculated for each ROI, except in ROIs having fewer than 18 unbound cells, where unbound cone density was calculated instead.

Statistical Analysis

Overtime trends in cone density were evaluated using random intercept models separately for each patient group (1°, 5°, and 10° T). Random intercept modeling assumes that image-to-image dependence is explained by subject's average level, whereas over time linear trends are the same across all subjects. For example, for subjects with high density values at earlier images, we anticipate higher density values at follow-up imaging. Thus, longitudinal subject-level linear trends only differ by intercepts but share the same slope. Because there was a suspicion that distribution of cone density was visually skewed to the right for some groups, we also performed statistical modeling on natural logarithmic scale. This logarithmic transformation made our variance less dependent of the outcome values. Cross-validation was used to calculate robust standard errors in each of these random effect models. Wald tests with these standard errors were used to evaluate statistical significance of overtime linear trends on original and log-transformed scales in the fitted random intercept models. R version 4.3.2 (Foundation for Statistical Computing) was used for fitting random intercept models.

Results

For the 19 individuals with ACHM (1 *CNGA3* and 18 *CNGB3*), the mean (± standard deviation) age at baseline was 21.6 ± 10.7 years (median, 17 years; range, 8−44 years). The mean (± standard deviation) follow-up time was 3.83 ± 2.93 years (median, 3.89 years; range, 0.46−8.66 years; Table S2, available at www.ophthalmologyscience.org). The number of visits, including the baseline visit, for each individual with usable data ranged from 2 to 8 visits. Six out of the 19 (31.58%) individuals (JC_10224, JC_10198, JC_10191, 10069, JC_10310, and JC_10151) had a follow-up visit >5 years. Four out of the 19 (21.05%) individuals (JC_10191, JC_10069, JC_10310, and JC_10151) had a follow-up visit >7 years.

Variable Changes in Cone Density Over Time

We were able to acquire and process analyzable parafoveal cone images using split-detector AOSLO for 187 of the 264 possible ROIs (70.8%). Table S2 details which ROIs were not included for each subject and each eccentricity, along with the reason for not including a given ROI (insufficient image quality or the same ROI location was not acquired). Of the 77 ROIs not included, 36 (46.8%) were due to the ROI having insufficient image quality to assess remnant cone structure, whereas 41 (53.2%) were due to that ROI location not having been acquired. A similar number of ROIs were excluded because of insufficient image quality at 1° T (n = 11), 5° T (n = 15), and 10° T (n = 10). In contrast, lack of acquisition was more common at 10° T (n = 30) that either 1° T (n = 0) or 5° T (n = 11). This is likely because rotational misalignments compound with increasing eccentricity.

From the 187 ROIs that were used in our analysis, 77 ROIs were from 19 individuals at 1° T, 62 ROIs were from 18 individuals at 5° T, and 48 ROIs were from 14 individuals at 10° T. At 1° T, the mean cone density across the total follow-up period was 11 100 cones/mm^2 (range, 4250−40 000 cones/mm^2). At 5° T, the mean cone density across the total follow-up period was 4520 cones/mm^2 (range, 1100−12 000 cones/mm^2). At 10° T, the mean cone density across the total follow-up period was 3400 cones/mm^2 (range, 200−7100 cones/mm^2). In comparison, these values are well below the previously reported normative histological values of 57 700, 19 700, 11 700, and 9120 cones/mm^2 at 1°, 3°, 7°, and 10° T, respectively.[20]

The linear mixed model at 1° T showed a significant decrease of 352 cones/mm^2 per year ($P = 0.0003$) (Fig 1A), which suggests cone loss throughout the follow-up period. The range of cone density change between baseline and the final follow-up visit at 1° T was −4520 to 2740 cones/mm^2. The linear mixed model at 5° T showed a decrease of 58 cones/mm^2 per year, although this was not significant ($P = 0.504$) (Fig 1B), which suggests that these cones were stable throughout the follow-up period (Fig 2). The range of cone density change between baseline and the final follow-up visit at 5° T was −2590 to 1560 cones/mm^2. The linear mixed model at 10° T showed a significant decrease of 139 cones/mm^2 per year ($P = 0.0188$) (Fig 1C), which suggests cone loss throughout the follow-up period (Fig 3). The range of cone density change between baseline and the final follow-up visit at 10° T was −1670 to 371 cones/mm^2. For the 100 × 100 μm ROIs used in this study, these changes in density correspond to an average decrease of between 0.5 and 4 cones per year, depending on the location.

Discussion

In this study, we observed a statistically significant decrease of 352 and 139 cones/mm^2 per year at 1° and 10° T, respectively, with a nonsignificant decrease of 58 cones/mm^2 per year at 5° T. Although our results show a decrease in parafoveal cone density, it is important to put these results in context with known repeatability of cone density

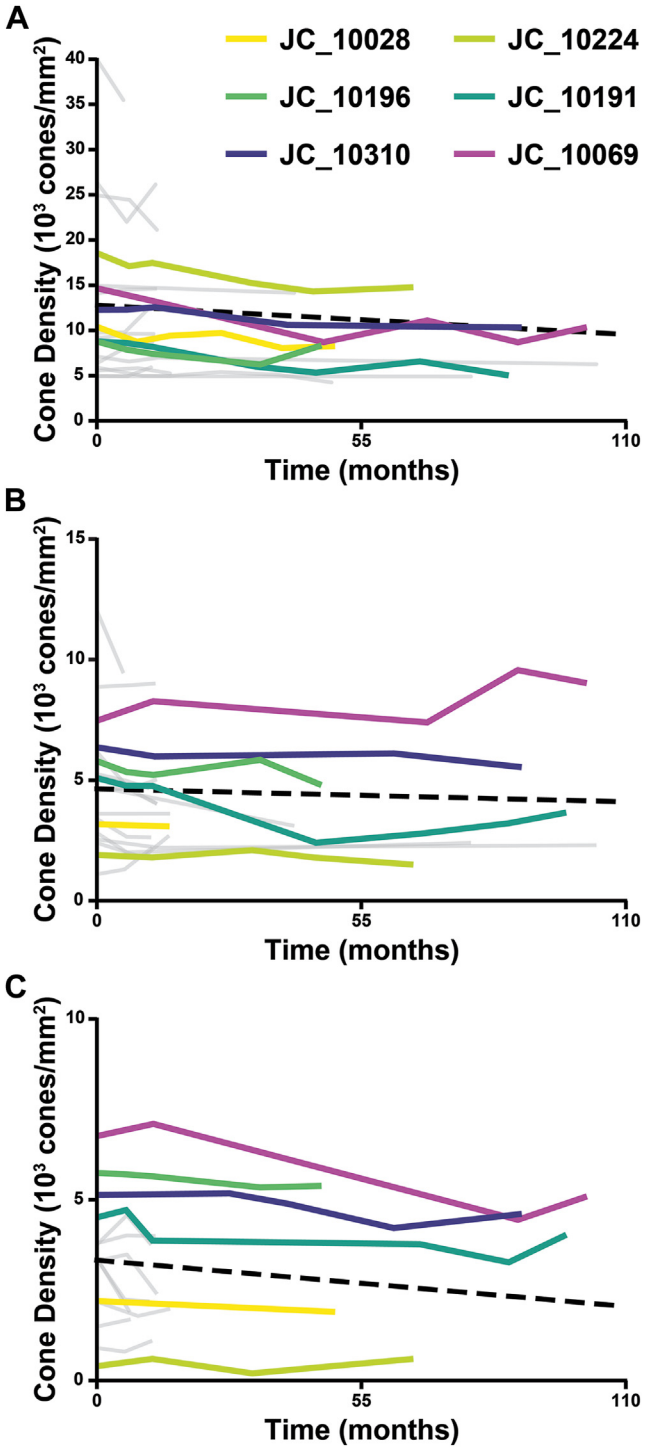

Figure 1. Longitudinal cone density over time for (**A**) the 19 individuals at 1° temporal, (**B**) the 18 individuals at 5° temporal, and (**C**) the 14 individuals at 10° temporal. Each line represents cone density values for a given individual. Colored lines represent individuals presented in Figures 2 and 3. Dotted line represents the linear mixed model showing the average change in cone density among all the individuals at that location. At 1° temporal there is an overall statistically significant decrease of 352 cones/mm^2 per year ($P = 0.0003$). At 5° temporal there a decrease of 58 cones/mm^2 per year that was not significantly significant ($P = 0.504$). At 10° temporal there is an overall statistically significant decrease of 139 cones/mm^2 per year ($P = 0.0188$). Raw data are available in Table S2

measures. In fact, the decrease in cone density are within the repeatability values Jackson et al[26] previously presented for normal retinas. Their longitudinal study measured cone density in normal retinas over time, which showed a 2-year mean (± standard deviation) cone density change of 100 ± 1800 cones/mm^2 at 350 µm (1.20°) and 1000 ± 2400

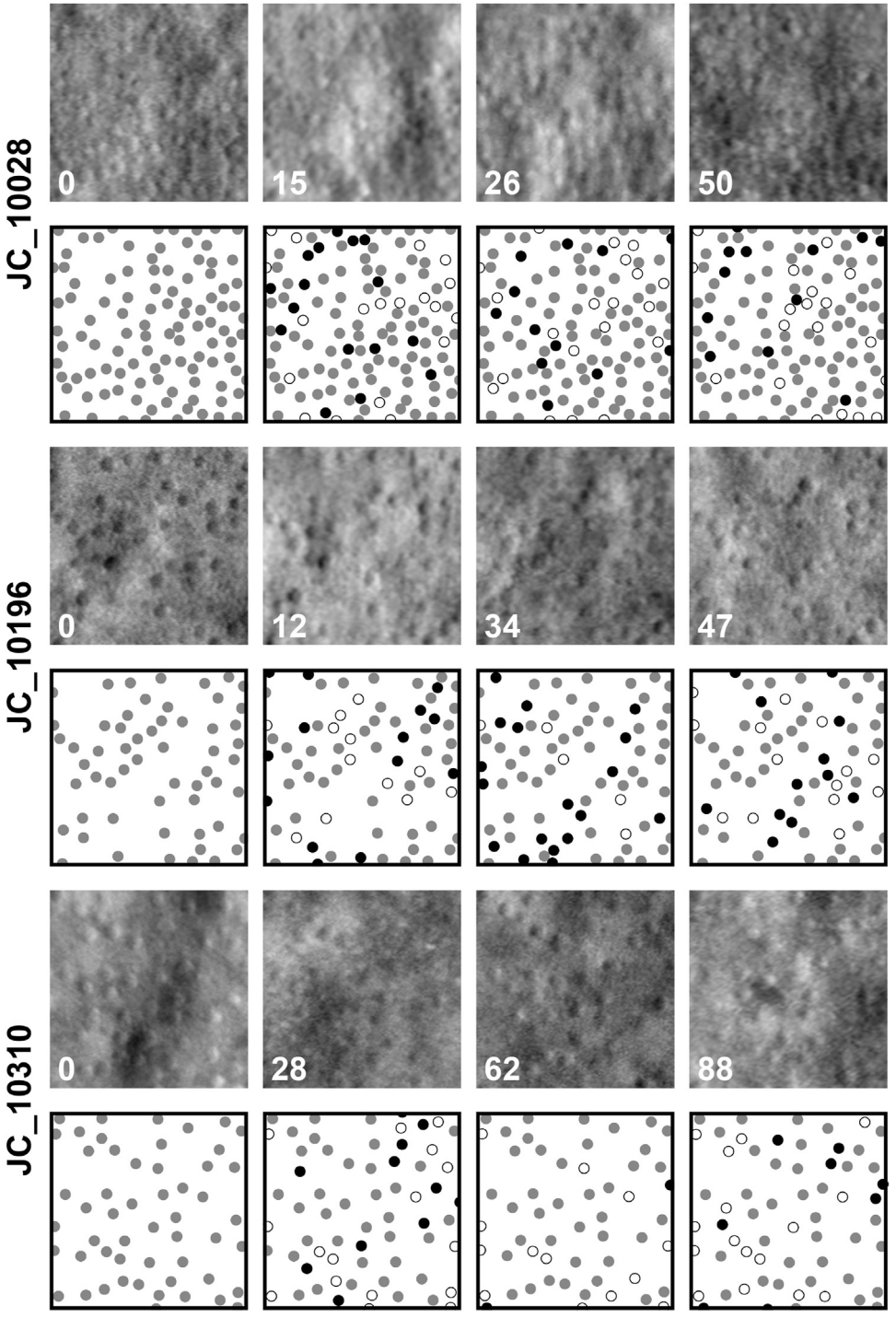

Figure 2. Examples of regions of interest (ROIs) showing no reduction in cone density over time. Shown below each ROI are the cones identified for each visit: gray fill = identified at baseline (and the respective follow-up visit); open circle = cone identified at baseline but not at the respective follow-up visit; and black fill = cone identified only at the respective follow-up visit. Images from JC_10028 at 1° temporal, JC_10196 at 5° temporal, and JC_10310 at 10° temporal. Despite differences in image quality and distortion, most cones are present throughout the follow-up period. Number in lower left of each image indicates number of months since baseline. ROIs are each 100 × 100 μm.

cones/mm^2 at 1500 μm (5.15°) in normal individuals.[26] Additionally, a previous study by Garrioch et al[27] examined repeatability of cone density measurements in normal individuals over a single imaging session. They found a repeatability of 2.7% or 1967 cones/mm^2. In other words, for 95% of pairs of observation, the difference between 2 measurements for the same individual would be <1967 cones/mm^2 at 190 μm (0.65°).[27] Taking these

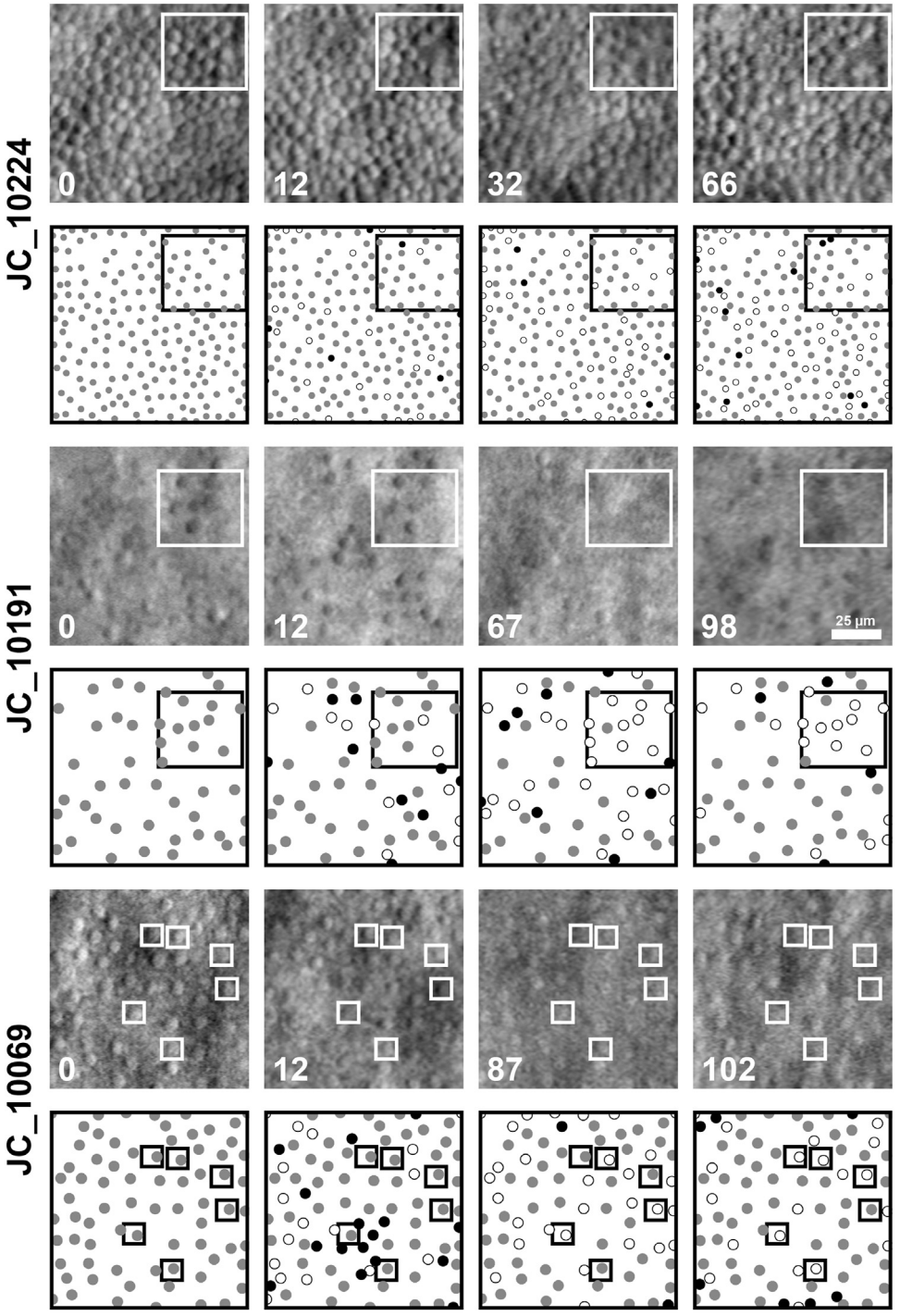

Figure 3. Examples of regions of interest (ROIs) showing reduction in cone density over time. Shown below each ROI are the cones identified for each visit: gray fill = identified at baseline (and the respective follow-up visit); open circle = cone identified at baseline but not at the respective follow-up visit; and black fill = cone identified only at the respective follow-up visit. Images from JC_10224 at 1° temporal show clear cone changes. Cones that are present at baseline disappear by 12 months and are still absent at 32 and 66 months (square insets). Images from JC_10191 at 5° temporal show variable cone loss across the follow-up period (square insets). Certain cones at baseline are present at 12 months, whereas some have begun to disappear. By 67 months, more of the outlined cones have disappeared. By the last follow-up period, almost all the cones have disappeared. Images from JC_10069 at 10° temporal shows various cones that are present at baseline and 12 months but begin to disappear by 87 months and some are still absent at 102 months (individual squares). The number in lower left of each image is the number of months since baseline. ROIs are each 100 × 100 µm.

findings from normal retinas into consideration, the decrease in cone density reported here may not be *clinically* meaningful. Of course, it is worth noting some methodological differences between the above studies. Garrioch et al[27] used confocal AOSLO images at a 55 × 55 μm ROI, whereas our study looked at ACHM individuals, with cone densities known to be lower than normal individuals, in the split imaging modality at a 100 × 100 μm ROI. In a study by Tanna et al[28] looking at individuals with Stargardt's, they found that there was no difference in cone density between the confocal and split-detector imaging modalities in 3 of the 4 graders. Additionally, they concluded that split-detection AOSLO provided a statistically significant higher reliability and repeatability of cone density measurements when compared with the confocal modality.[28] Although the size of the ROI is known to influence cone density, the study by Zaleska-Żmijewska et al[29] found that there was not a statistical difference in cone density between 50 × 50 μm and 100 × 100 μm ROIs. An additional point is that we analyzed the ROIs in a randomized masked fashion to mirror what might be done in a clinical trial. Unmasked side-by-side examination of images from different time points might aide in the interpretation of cone structure at a given time point, which might provide a more accurate picture of biological changes in ACHM. That said, because the focus of our study was to provide data that could ultimately be used for comparison in individuals receiving gene replacement therapy, we believed it best to adopt an analytical approach similar to what would be used in a trial.

Because age-related changes can confound the interpretation of our results, it is also imperative to discern the difference between disease progression and normal age-related changes. In a cross-sectional AOSLO imaging study conducted by Park et al,[30] they found a negative correlation between cone density and age, although the correlation was not statistically significant. A different cross-sectional AOSLO imaging study conducted by Song et al[31] showed that cone density is statistically lower within 0.45 mm of the fovea in older (50−65 years old) compared with younger (22−35 years old) individuals. More recently, Reumueller et al[32] used adaptive optics OCT to show a statistically significant decrease in cone density of 10 cones/mm^2 per year. Although our study showed a statistically significant decrease in cone density, it is difficult to discern if our changes in cone density changes are attributable to disease progression rather than natural aging. Histologically, Curcio et al[33] found that cone density is stable during adulthood, but rod density decreases by 30% by the ninth decade of life, with an average loss of 684 rods/mm^2 per year. Alternatively, histological studies conducted by Panda-Jonas et al,[34] found that, although rods were affected more than cones, both cones and rods declined with age with a large decline in parafoveal regions as early as 2 to 5 mm away from the fovea, but most prominent decline 5 to 8 mm away from the fovea. They predicted a steady loss of 236 rods/mm^2 per year and a 5.90 cones/mm^2 per year or a 37% decline in rods and a 18% decline in cones in a 100-year lifespan.[34] Similarly, Gao and Hollyfield[35] also concluded rods are more vulnerable to cones with increasing age and photoreceptor loss accompanying age was less pronounced in the fovea when compared with the periphery. Because ACHM is a congenital condition affecting proteins expressed in cone photoreceptors, the remaining visual functions in patients with ACHM is primarily mediated by the normally functioning rod photoreceptors. Therefore, any natural/normal loss of rod photoreceptors could contribute to perceived progression of ACHM. Further AOSLO imaging studies in normal individuals may be necessary to help interpret age-related changes in the overall photoreceptor mosaic (i.e., determine whether any observed changes are due to normal aging or are a part of the ACHM disease sequence).

There are some limitations to our study. First, only individuals with a successful record of AOSLO imaging were followed (because of resource limitations). Previous estimates suggest a success rate of around 50% in this population, and this issue of selection bias may misrepresent the degree of remnant cone structure in ACHM.[36] This may also impact longitudinal measures, so our observations may not necessarily extend to other ACHM populations. Second, we relied on the presence of individual cones at locations with decent quality images for alignment of AOSLO montages. Nystagmus, poor fixation, fatigue, and other factors for a portion of individuals at follow-up time points resulted in the same area on follow-up not always being imaged or, if it was imaged, it was not always of sufficient quality for analysis. The focus offset between rods in the confocal channel and cones in the split-detection channel contributes to this issue of "quality," as the fully processed split-detection image was not visible to the operator in real-time. Regardless of the reason, there were fewer ROIs at follow-up despite quantifiable ROIs at earlier time points for some individuals (see Table S2). Thus, real changes in cone structure at locations excluded on follow-up could have been missed. Our experience was similar to previous studies that had challenges acquiring consistent and analyzable image quality over time.[7,14] Future opportunities to implement eye-tracking tools on AOSLO devices might aid in imaging challenging patient populations, and use of OCT to prescreen patients could potentially increase overall yield.[37] Third, many individuals had a short follow-up time as the mean follow-up time was 3.83 years (median, 3.89 years), which might not be long enough if ACHM is a slowly progressive condition. Previous longitudinal OCT studies had follow-up times ranging from 1.07 to 5.7 years,[10,12−17] although only 3 of these studies had a longer mean follow-up time than that of our study.[15−17] Additionally, 6 of our 19 (31.58%) individuals were followed for >5 years, and 4 of our 19 (21.05%) individuals had follow-up visits >7 years. Lastly, most individuals in our study had *CNGB3*-associated ACHM, with only one individual with *CNGA3*-associated ACHM. The progression and phenotypic changes for other genotypes causing ACHM, might be different. We already know that *GNAT2*- and *ATF6*-associated ACHM have a different phenotype compared with *CNGA3*- and *CNGB3*-associated ACHM.[4,38−40] Our cohort did not include many children for which we could get analyzable images over time. As

nystagmus is shown to decrease with age in some individuals,[2] it is possible that AOSLO image quality could improve. As such, continued evaluation of these patients is worthwhile even when initial imaging is unsuccessful.

With respect to future longitudinal studies involving AOSLO imaging, our study offers some important insights. First, given the small field of view used in most AOSLO systems, real-time alignment to a baseline montage is critical to ensure the same retinal locations are imaged over time. This will ensure the inclusion of the greatest number of possible ROIs in a longitudinal study. Second, it is important to develop uniform training for individuals performing image acquisition as laboratory and clinic personnel can change over the course of a long study. We were not able to use the same operator over time for each individual, with 29 unique individuals being involved in image acquisition (see Table S2). In our experience, operator expertise can result in variability in image quality and success rate, especially in challenging patient populations such as ACHM. We have a fairly robust internal training program, which aligns with the observation that there was no obvious trend of ROI exclusion due to image quality issues being associated with specific imagers (see Table S2). Regardless, future studies should include a form of imager certification to ensure consistency within the study/trial. Finally, identification of cones and cone density measurements relied on a semiautomatic process. Nonautomated, manual identification of photoreceptors relies heavily on observer experience and subjective interpretation of structural features in split-detector images.[41] Both factors can impact consistency of cone identification. This variability was attempted to be minimized in our study 2 ways. First, by having a single, experienced observer for all initial measurements. Second, cone density was reviewed by a second observer and then rereviewed with both observers together. Indeed, previous studies have shown good intraobserver repeatability of manual cone density measurements for both individuals with normal vision and individuals with ACHM.[14,42] Whereas, interobserver studies of cone density measurements in ACHM have shown poor reproducibility.[41] Although previous studies showed intraobserver cone density measurements were repeatable, the exact cones identified can vary. In our study, this can be seen as specific cones identified differed across the study period, yet the cone density remained stable (see Fig 2). Future longitudinal studies may benefit from further advances in automation of cell detection in split-detector AOSLO images, which would help standardize cone identification and cone density measurements.[43,44]

In conclusion, we observed small reductions in parafoveal cone density in ACHM, although we propose that these changes are not clinically meaningful in the context of previous longitudinal and repeatability studies in normal individuals. Our results are consistent with ACHM being a stable or a very slowly progressing condition (at least with respect to cone structure), which aligns with numerous prior results. Such data will be useful in interpreting results from prior and ongoing gene therapy studies in ACHM.[45]

Footnotes and Disclosures

Originally received: September 3, 2024.
Final revision: February 21, 2025.
Accepted: March 10, 2025.
Available online: March 14, 2025. Manuscript no. XOPS-D-24-00350R2.

[1] School of Medicine, Medical College of Wisconsin, Milwaukee, Wisconsin.

[2] Department of Ophthalmology and Visual Sciences, Medical College of Wisconsin, Milwaukee, Wisconsin.

[3] Bascom Palmer Eye Institute, University of Miami, Miami, Florida.

[4] Department of Ophthalmology and Visual Sciences, University of Illinois Chicago, Chicago, Illinois.

[5] Chicago College of Optometry, Midwestern University, Downers Grove, Illinois.

[6] The Chicago Lighthouse, Chicago, Illinois.

[7] Casey Eye Institute, Oregon Health & Science University, Portland, Oregon.

[8] Retina Foundation of the Southwest, Dallas, Texas.

[9] Vitreo Retinal Associates, Gainesville, Florida.

[10] Division of Biostatistics, Medical College of Wisconsin, Milwaukee, Wisconsin.

[11] Department of Cell Biology, Neurobiology and Anatomy, Medical College of Wisconsin, Milwaukee, Wisconsin.

*N.C. and K.M.L. contributed equally to this work.

†Current affiliation: Genentech Inc., South San Francisco, California.

Presented at the Association for Research in Vision and Ophthalmology (ARVO) annual meeting, May 5-9, 2024, Seattle, Washington.

Disclosures:

All authors have completed and submitted the ICMJE disclosures form.

The authors made the following disclosures:

K.M.L.: Financial support — National Institutes of Health/National Eye Institute grant F32EY029148-Medical College of Wisconsin; Stock or stock options — Roche; Employee — Genentech.

B.L.L.: Grant support — Atsena, Biogen, Endogena, Nanoscope, Ocugen, Spark, Stoke; Consultant — Biogen, BlueRock, Janssen, Lexitas, Stoke.

M.E.P.: Grant support — AGTC; Consultant — AGTC/Beacon; Meetings and travel support — Beacon.

C.N.K.: Grant support — AGTC/Beacon Therapeutics (clinical trial funding).

J.C.: Financial support — NIH R01EY017607, NIH UL1TR001436, NIH C06RR016511 (to institution); Consultant — Translational Imaging Innovations.

The other authors have no proprietary or commercial interest in any materials discussed in this article.

Supported in part by the National Eye Institute of the National Institutes of Health under award numbers R01EY017607, P30EY010572, R24EY022023, and F32EY029148; by the National Center for Advancing Translational Sciences under award number UL1TR001436; unrestricted grant from Research to Prevent Blindness to CEI; and the Foundation Fighting Blindness (USA). This investigation was conducted in part in a facility constructed with support from a Research Facilities Improvement Program (grant number C06RR016511) from the National Center for Research Resources, NIH. The sponsors and funding organization had no role in the design or conduct of this research. The content is solely the

responsibility of the authors and does not necessarily represent the official views of the National Institutes of Health. Additional support was provided by the Gene and Ruth Posner Foundation (Milwaukee, Wisconsin) and AchromaCorp (Oak Hills, Pennsylvania).

Support for Open Access publication was provided by the Medical College of Wisconsin.

HUMAN SUBJECTS: Human subjects were included in this study. The research study was approved by Institutional Review Board at the Medical College of Wisconsin (PRO00027165). All research adhered to the tenets of the Declaration of Helsinki. All participants provided informed consent.

No animal subjects were used in this study.

Author Contributions:

Conception and design: Chen, Litts, Langlo, Lam, Fishman, Collison, Pennesi, Kay, Carroll

Data collection: Chen, Litts, Nikezic, Higgins, Carroll

Analysis and interpretation: Chen, Litts, Nikezic, Langlo, Higgins, Tarima, Carroll

Obtained funding: Litts, Carroll

Overall responsibility: Chen, Litts, Carroll

Abbreviations and Acronyms:
ACHM = achromatopsia; **AOSLO** = adaptive optics scanning light ophthalmoscope; **EZ** = ellipsoid zone; **ONL** = outer nuclear layer; **ROI** = region of interest; **SD** = standard deviation; **T** = temporal.

Keywords:
Achromatopsia, Adaptive optics scanning light ophthalmoscope (AOSLO), Cone photoreceptor, Retina, Retina imaging.

Correspondence:
Joseph Carroll, PhD, 925 N 87th St, Milwaukee, WI 53226-0509. E-mail: jcarroll@mcw.edu.

References

1. Kohl S, Baumann B, Rosenberg T, et al. Mutations in the cone photoreceptor G-protein alpha-subunit gene *GNAT2* in patients with achromatopsia. *Am J Hum Genet*. 2002;71:422−425.
2. Kohl S, Varsanyi B, Antunes GA, et al. *CNGB3* mutations account for 50% of all cases with autosomal recessive achromatopsia. *Eur J Hum Genet*. 2005;13:302−308.
3. Kohl S, Coppieters F, Meire F, et al. A nonsense mutation in *PDE6H* causes autosomal-recessive incomplete achromatopsia. *Am J Hum Genet*. 2012;91:527−532.
4. Kohl S, Zobor D, Chiang WC, et al. Mutations in the unfolded protein response regulator *ATF6* cause the cone dysfunction disorder achromatopsia. *Nat Genet*. 2015;47:757−765.
5. Merino D, Duncan JL, Tiruveedhula P, Roorda A. Observation of cone and rod photoreceptors in normal subjects and patients using a new generation adaptive optics scanning laser ophthalmoscope. *Biomed Opt Express*. 2011;2:2189−2201.
6. Genead MA, Fishman GA, Rha J, et al. Photoreceptor structure and function in patients with congenital achromatopsia. *Invest Ophthalmol Vis Sci*. 2011;52:7298−7308.
7. Langlo CS, Patterson EJ, Higgins BP, et al. Residual foveal cone structure in *CNGB3*-associated achromatopsia. *Invest Ophthalmol Vis Sci*. 2016;57:3984−3995.
8. Georgiou M, Litts KM, Kalitzeos A, et al. Adaptive optics retinal imaging in *CNGA3*-associated achromatopsia: retinal characterization, interocular symmetry, and intrafamilial variability. *Invest Ophthalmol Vis Sci*. 2019;60:383−396.
9. Thiadens AA, Somervuo V, van den Born LI, et al. Progressive loss of cones in achromatopsia: an imaging study using spectral-domain optical coherence tomography. *Invest Ophthalmol Vis Sci*. 2010;51:5952−5957.
10. Thomas MG, McLean RJ, Kohl S, et al. Early signs of longitudinal progressive cone photoreceptor degeneration in achromatopsia. *Br J Ophthalmol*. 2012;96:1232−1236.
11. Sundaram V, Wilde C, Aboshiha J, et al. Retinal structure and function in achromatopsia: implications for gene therapy. *Ophthalmology*. 2014;121:234−245.
12. Aboshiha J, Dubis AM, Cowing J, et al. A prospective longitudinal study of retinal structure and function in achromatopsia. *Invest Ophthalmol Vis Sci*. 2014;55:5733−5743.
13. Grissim G, Walesa A, Follett HM, et al. Longitudinal assessment of OCT-based measures of foveal cone structure in achromatopsia. *Invest Ophthalmol Vis Sci*. 2024;65:16.
14. Langlo CS, Erker LR, Parker M, et al. Repeatability and longitudinal assessment of foveal cone structure in *CNGB3*-associated achromatopsia. *Retina*. 2017;37:1956−1966.
15. Hirji N, Georgiou M, Kalitzeos A, et al. Longitudinal assessment of retinal structure in achromatopsia patients with long-term follow-up. *Invest Ophthalmol Vis Sci*. 2018;59:5735−5744.
16. Brunetti-Pierri R, Karali M, Melillo P, et al. Clinical and molecular characterization of achromatopsia patients: a longitudinal study. *Int J Mol Sci*. 2021;22:1681.
17. Triantafylla M, Papageorgiou E, Thomas MG, et al. Longitudinal evaluation of changes in retinal architecture using optical coherence tomography in achromatopsia. *Invest Ophthalmol Vis Sci*. 2022;63:6.
18. Katta M, Georgiou M, Singh N, et al. Longitudinal imaging of the foveal cone mosaic in *CNGA3*-associated achromatopsia. *Invest Ophthalmol Vis Sci*. 2024;65:6.
19. Davis JL, Gregori NZ, MacLaren RE, Lam BL. Surgical technique for subretinal gene therapy in humans with inherited retinal degeneration. *Retina*. 2019;39(suppl 1):S2−S8.
20. Curcio CA, Sloan KR, Kalina RE, Hendrickson AE. Human photoreceptor topography. *J Comp Neurol*. 1990;292:497−523.
21. Litts KM, Georgiou M, Langlo CS, et al. Interocular symmetry of foveal cone topography in congenital achromatopsia. *Curr Eye Res*. 2020;45:1257−1264.
22. Dubra A, Sulai Y, Norris JL, et al. Noninvasive imaging of the human rod photoreceptor mosaic using a confocal adaptive optics scanning ophthalmoscope. *Biomed Opt Express*. 2011;2:1864−1876.
23. Salmon AE, Cooper RF, Langlo CS, et al. An automated reference frame selection (ARFS) algorithm for cone imaging with adaptive optics scanning light ophthalmoscopy. *Transl Vis Sci Technol*. 2017;6:9.
24. Chen M, Cooper RF, Han GK, et al. Multi-modal automatic montaging of adaptive optics retinal images. *Biomed Opt Express*. 2016;7:4899−4918.
25. Chen M, Cooper RF, Gee JC, et al. Automatic longitudinal montaging of adaptive optics retinal images using constellation matching. *Biomed Opt Express*. 2019;10:6476−6496.
26. Jackson K, Vergilio GK, Cooper RF, et al. A 2-year longitudinal study of normal cone photoreceptor density. *Invest Ophthalmol Vis Sci*. 2019;60:1420−1430.

27. Garrioch R, Langlo C, Dubis AM, et al. Repeatability of *in vivo* parafoveal cone density and spacing measurements. *Optom Vis Sci*. 2012;89:632−643.
28. Tanna P, Kasilian M, Strauss R, et al. Reliability and repeatability of cone density measurements in patients with Stargardt disease and *RPGR*-associated retinopathy. *Invest Ophthalmol Vis Sci*. 2017;58:3608−3615.
29. Zaleska-Żmijewska A, Wawrzyniak ZM, Ulińska M, et al. Human photoreceptor cone density measured with adaptive optics technology (rtx1 device) in healthy eyes: standardization of measurements. *Medicine (Baltimore)*. 2017;96:e7300.
30. Park SP, Chung JK, Greenstein V, et al. A study of factors affecting the human cone photoreceptor density measured by adaptive optics scanning laser ophthalmoscope. *Exp Eye Res*. 2013;108:1−9.
31. Song H, Chui TY, Zhong Z, et al. Variation of cone photoreceptor packing density with retinal eccentricity and age. *Invest Ophthalmol Vis Sci*. 2011;52:7376−7384.
32. Reumueller A, Schmidt-Erfurth U, Salas M, et al. Three-dimensional adaptive optics-assisted visualization of photoreceptors in healthy and pathologically aged eyes. *Invest Ophthalmol Vis Sci*. 2019;60:1144−1155.
33. Curcio CA, Millican CL, Allen KA, Kalina RE. Aging of the human photoreceptor mosaic: evidence for selective vulnerability of rods in central retina. *Invest Ophthalmol Vis Sci*. 1993;34:3278−3296.
34. Panda-Jonas S, Jonas JB, Jakobczyk-Zmija M. Retinal photoreceptor density decreases with age. *Ophthalmology*. 1995;102:1853−1859.
35. Gao H, Hollyfield JG. Aging of the human retina. Differential loss of neurons and retinal pigment epithelial cells. *Invest Ophthalmol Vis Sci*. 1992;33:1−17.
36. Litts KM, Woertz EN, Wynne N, et al. Examining whether AOSLO-based foveal cone metrics in achromatopsia and albinism are representative of foveal cone structure. *Transl Vis Sci Technol*. 2021;10:22.
37. Litts KM, Woertz EN, Georgiou M, et al. Optical coherence tomography artifacts are associated with adaptive optics scanning light ophthalmoscopy success in achromatopsia. *Transl Vis Sci Technol*. 2021;10:11.
38. Dubis AM, Cooper RF, Aboshiha J, et al. Genotype-dependent variability in residual cone structure in achromatopsia: toward developing metrics for assessing cone health. *Invest Ophthalmol Vis Sci*. 2014;55:7303−7311.
39. Mastey RR, Georgiou M, Langlo CS, et al. Characterization of retinal structure in *ATF6*-associated achromatopsia. *Invest Ophthalmol Vis Sci*. 2019;60:2631−2640.
40. Georgiou M, Singh N, Kane T, et al. Photoreceptor structure in *GNAT2*-associated achromatopsia. *Invest Ophthalmol Vis Sci*. 2020;61:40.
41. Abozaid MA, Langlo CS, Dubis AM, et al. Reliability and repeatability of cone density measurements in patients with congenital achromatopsia. *Adv Exp Med Biol*. 2016;854:277−283.
42. Liu BS, Tarima S, Visotcky A, et al. The reliability of parafoveal cone density measurements. *Br J Ophthalmol*. 2014;98:1126−1131.
43. Cunefare D, Langlo CS, Patterson EJ, et al. Deep learning based detection of cone photoreceptors with multimodal adaptive optics scanning light ophthalmoscope images of achromatopsia. *Biomed Opt Express*. 2018;9:3740−3756.
44. Davidson B, Kalitzeos A, Carroll J, et al. Automatic cone photoreceptor localisation in healthy and Stargardt afflicted retinas using deep learning. *Sci Rep*. 2018;8:7911.
45. Michaelides M, Hirji N, Wong SC, et al. First-in-human gene therapy trial of AAV8-hCARp.hCNGB3 in adults and children with *CNGB3*-associated achromatopsia. *Am J Ophthalmol*. 2023;253:243−251.